RNG k-ε modelling and mobilization experiments of loss of vacuum in small tanks for nuclear fusion safety applications

P.Gaudio, A.Malizia, I.Lupelli

Abstract— The objective of this work concerns the RNG k-ε modelling and mobilization experiments of loss of vacuum in small tanks for nuclear fusion safety applications. Activated dust mobilization during a Loss of Vacuum Accidents (LOVA) is one of the safety concerns for the International Thermonuclear Experimental Reactor (ITER). Intense thermal loads in fusion devices occur during plasma disruptions, Edge Localized Modes (ELM) and Vertical Displacement Events (VDE). They will result in macroscopic erosion of the plasma facing materials and consequent accumulation of activated dust into the ITER Vacuum Vessel (VV). These kind of events can cause the dust leakage outside the VV that represents a high radiological risk for the workers and the population. A small facility, Small Tank for Aerosol Removal and Dust (STARDUST), was set up at the ENEA Frascati laboratories to perform experiments concerning the dust mobilization in a volume with the initial condition similar to those existing in ITER VV. The aim of this work was to reproduce a low pressurization rate (300 Pa/s) LOVA event in a vacuum vessel due to a small air leakage for two different positions of the leak, at the equatorial port level and at the divertor port level, in order to evaluate the influence of obstacles and walls temperature on dust resuspension during both maintenance (MC) and accident conditions (AC) (Twalls=25°C MC, 110°C AC). The dusts used were

- tungsten (W);
- stainless steel 316 (SS316);
- carbon (C).

similar to those produced inside the vacuum chamber in a fusion reactor when the plasma facing materials vaporize due to the high energy deposition. The experimental campaign has been carried out by introducing inside STARDUST facility an obstacle to simulate the presence of objects, like divertor.
In the obstacle a slit was cut to simulate the limiter-divertor gap inside ITER VV.
The velocity magnitude in STARDUST was investigated in order to map the velocity field by means of a punctual capacitive transducer placed inside STARDUST without obstacles.
In this paper experimental campaign results are shown in order to investigate how the divertor and limiter-divertor gap influence dust mobilization into a VV. A two-dimensional (2D) modelling of STARDUST was made with the CFD commercial code FLUENT, in order to get a preliminary overview of the fluid dynamics behaviour during a LOVA event and to justify the mobilization data. Besides a numerical model was developed to compare numerical results with experimental ones.

***Keywords*—**Dust mobilization, nuclear fusion safety, LOVA, CFD.

I. Introduction

Fluid-solid flow phenomena is an interdisciplinary research area with great technological, commercial and medical importance [1]. A recognized safety issue for future fusion reactors (like ITER) fueled with deuterium and tritium is the generation of sizeable quantities of dust [2-4]. The loss of coolant accidents (LOCA), loss of coolant flow accidents (LOFA) and loss of vacuum accidents (LOVA) are types of accidents that may jeopardize the components and the plasma vessel integrity and cause dust mobilization, risky for workers and public [5]. In order to analyze this problems a small facility STARDUST was set up at University of Rome "Tor Vergata" in collaboration with the ENEA Frascati National Laboratory Fusion Technology Department that reproduce a LOVA event postulated in ITER. Several experiments have been conducted with STARDUST facility in order to reproduce a low pressurization rate (300 Pa/s due to a 0,02 m^2 wide breach defined by Generic Site Specific Report (GSSR) [6]) LOVA event in ITER for two different positions of the leak, at the equatorial port level and at the divertor port level, in order to perform:

- Dust resuspension experiments (with tungsten (W), stainless steel (SS) and carbon (C), similar to those produced inside the vacuum chamber in a fusion reactor. These experiments are carried out with STARDUST facility in order to analyze both the influence of obstacles like the divertor or particular geometrical configuration inside the VV (like the LDG1), and the influence of temperature on dust resuspension during maintenance and operative conditions. All the experimental results will be

P.Gaudio is with University of Rome "Tor Vergata", Faculty of Engineering, Department of Mechanical Engineering, Quantum Electronics and Plasma Physics Research Group, Via del Politecnico 1, 00133 Rome, Italy (corresponding author phone: 0039 0672597209; fax: 0039 0672597207; e-mail: gaudio@ing.uniroma2.it).

A.Malizia is with University of Rome "Tor Vergata", Faculty of Engineering, Department of Mechanical Engineering, Quantum Electronics and Plasma Physics Research Group, Via del Politecnico 1, 00133 Rome, Italy (corresponding author phone: 0039 0672597196; fax: 0039 0672597207; e-mail: malizia@ing.uniroma2.it).

I.Lupelli is with University of Rome "Tor Vergata", Faculty of Engineering, Department of Mechanical Engineering, Quantum Electronics and Plasma Physics Research Group, Via del Politecnico 1, 00133 Rome, Italy (corresponding author phone: 0039 0672597196; fax: 0039 0672597207; e-mail: ivan.lupelli@uniroma2.it).

analyzed and discussed;

- Punctual velocity evaluation in order to study the flow field in case of LOVA and its connection with dust mobilization phenomena.

FLUENT was used to simulate the flow behavior for the same LOVA scenarios used during the experimental tests. For the design and licensing of the nuclear fusion power plant Computational Fluid Dynamics (CFD) codes are considered an essential tool [7]. Therefore, experimental activities and numerical simulation campaigns have been carried out in strong correlation in order both to understand the capabilities of computational codes and to predict correctly the characteristics of the flows during a LOVA event. A model which could predicts the velocity magnitude for different conditions during a LOVA event in the whole domain is an important tool to support regulatory approval of a fusion device. A two-dimensional (2D) modeling of STARDUST, made with the CFD commercial code FLUENT, will be carried out. A comparison of the experiments data in STARDUST with the numerical simulation results will be shown for CFD code validation. For validation purposes, the CFD simulation data will be extracted at the same locations as the experimental data will be collected. In this paper the computer-simulation data and the comparison with data collected during the laboratory studies will be discussed and presented in order to evaluate a first resuspension numerical model.

II. Experimental set-up

STARDUST Facility and LOVA reproduction

The main dimensions of STARDUST(Fig.1) are reported in the following table (Tab.1):

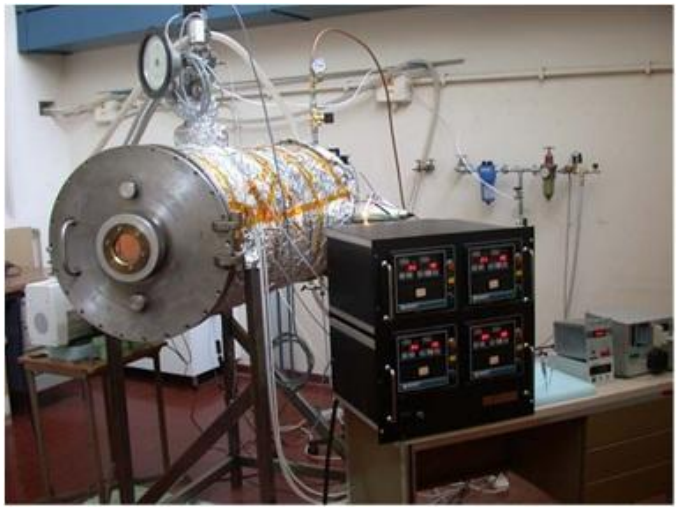

Fig. 1 STARDUST facility

External length of the tank (mm)	920
External diameter of the tank (mm)	506
External diameter of the lids (mm)	570
Thickness of the tank's wall (mm)	5
Thickness of the lid (mm)	14
Quartz lateral windows : distance from the pipe inlet (center of the window) (mm)	182
Diameter of the lateral quartz windows (mm)	84
Diameter of the frontal quartz window in the mobile lid (mm)	79
Internal volume of the tank (m^3)	0,17

Tab. 1 main dimensions of STARDUST [8,9]

A labview software has been developed in order to control all the hardware and to storage automatically the data. These are the steps of program:

- Switch on the heaters (only for 110 °C test)
- The pneumatic-valve is open;
- The vacuum pump is turned on;
- The user can monitor the temperature and pressure conditions and the flow rate during the achievement of the test initial conditions;
- When the initial conditions are reached the program automatically closes the pneumatic-valve and vacuum pump is turned off.
- The inlet section (A or B which represent respectively a window leakage at equatorial port level and at the divertor port level in a fusion plant (Fig.2)) is selected as the path-file for the data storage;
- The air mass flow is set to 27 l/min in order to reproduce a 300 Pa/s LOVA event and feed valve is open.

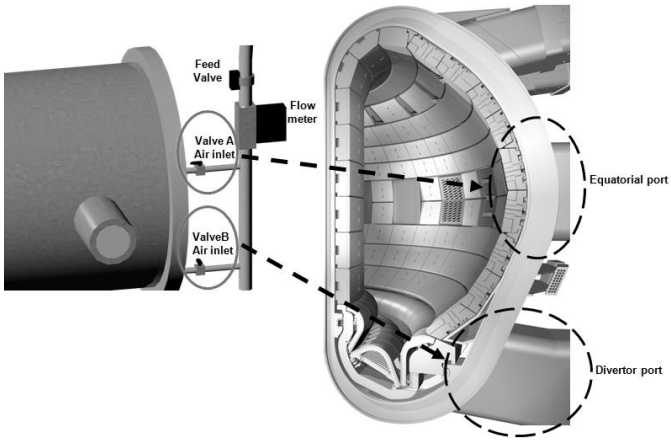

Fig. 2 STARDUST facility

- The acquisition starts, and the data are stored at 50 Hz;
- When the internal pressure equals the external one the program automatically allows the closure of flow meter and the experiment is over.

Figure 3 shows a schematic layout of the LOVA simulation experiment made by STARDUST.

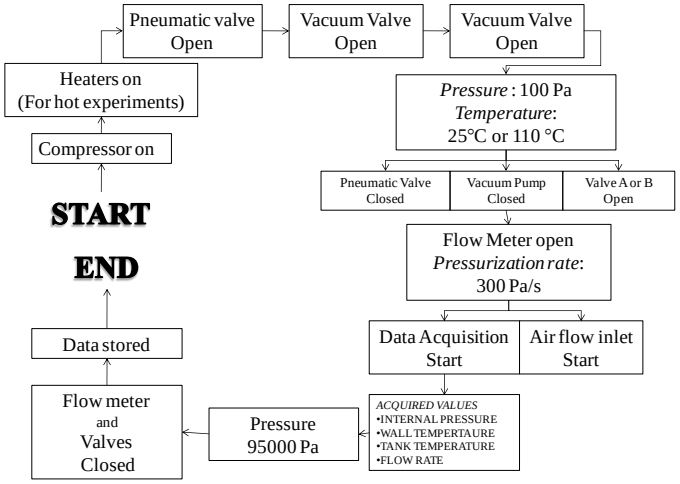

Fig. 3 LOVA simulation made by STARDUST

Quantitative measurements of dust resuspension

In ITER VV there are several structures that could influence the dust mobilization during a LOVA, such as the divertor cassettes (Figure 4b). In order to estimate their effects an obstacle was placed into STARDUST. The obstacle is a stainless steel cot and it is provided with a bridge that aims to reproduce the divertor dome (Figure 4a). After a first set of experiments, a slit on the obstacle has been made in order to analyze the effects of a gap if the air inlet occurs between the limiter and the divertor (LDG - Limiter Divertor Gap) in ITER by the comparison of dust mobilizated in the experiments with and without the slit on the obstacle.

The main geometrical characteristic of slit (dimension in mm) are reported in Figure 4c, the height of the slit is 2,5 mm and the width is 290 mm.

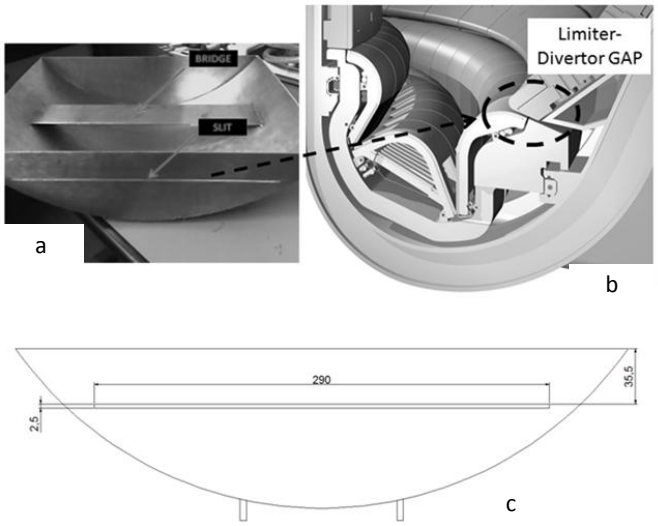

Fig. 4 The obstacle: in evidence the bridge representing ITER divertor dome and the slit simulating the LDG in ITER

The type of dust used (W, C, SS316) is similar to that it is possible to find inside the vacuum chamber of a fusion facility, when, the plasma facing materials vaporize for the high energy deposition due to the disruptions [8]. Scanning Electron Microscope (SEM) analysis has been carried out for characterizing the commercial dust used for the experiments[8]. The dust mean diameter measured was 0.3-0.5 μm for W, 20-30 μm for SS316 and 4-5 μm for C. The dust size distributions is shown in figure 5 for C (received from FZK), in figure 6 for W (treated by carbon deposition, 2.0-3.0 nm) and in figure 7 for SS316 (treated by carbon deposition, 2.0-3.0 nm). The results of the SEM scanning revealed a size distribution of the dust different from those declared by the commercial companies, that was 0.6-0.9 micron for W and 45 micron for SS316 against the 0.3-0.5 micron detected by the SEM for the W and 15-30 micron for the SS316, respectively [8].

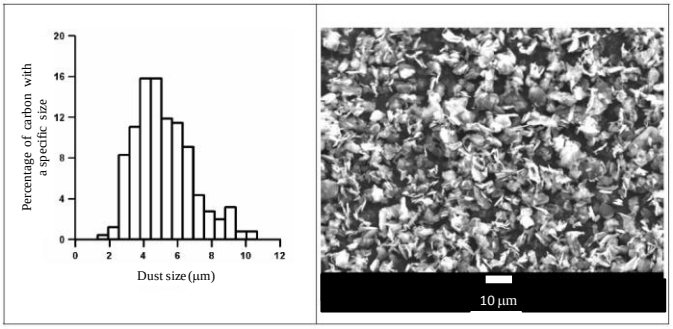

Fig. 5 Distribution and SEM image of carbon dust [8]

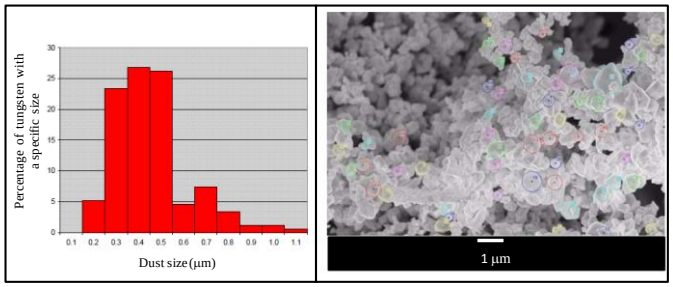

Fig. 6 Distribution and SEM image of tungsten dust [8]

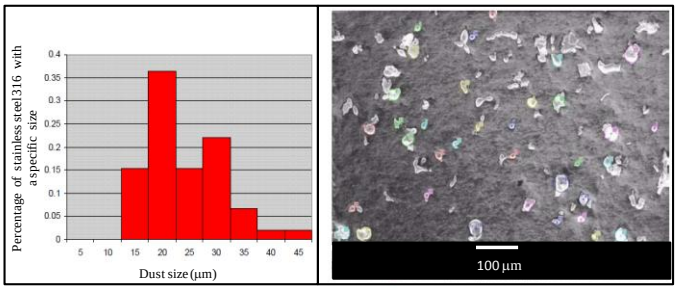

Fig. 7 Distribution and SEM image of stainless steel 316 dust [8]

Between the dust's sizes commercially available, those similar to the dusts generated in the disruptions phenomena has been chosen [8]. While the W and the C grains had the tendency to agglomerate each other, the stainless steel, being of bigger size and with a high specific weight, remained well separated between them. This behavior was significant in the piles preparation for the experiments, because it was possible to form similar heaps for the all the tests with the stainless steel, while the tungsten piles and carbon piles were different for each test [8]. This feature has an influence in the mobilization rate. The effect of the humidity in the agglomeration has to be excluded, because of the vacuum condition in the tank [8]. The dust was placed on a tray (area 25 cm^2) in order to reproduce a superficial density as expected in ITER (Figure 8). In these experiments the dust has been deposited on the tray using a sieve to avoid heaps.

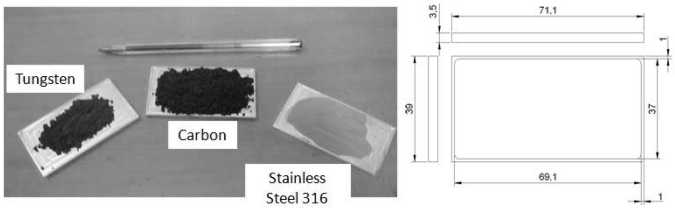

Fig. 8 Images of dust used and main dimension of tray (in mm) [8]

The amount of dust used was: 0.5 g for W and SS316, 0.2 g for C. The experiments have been performed in the following configurations:

a) Tray with dust (figure 9);
b) Tray without the obstacle, in the bottom part of the tank (figure 9);
c) Tray under the obstacle at the bottom part of the tank (figure 9);
d) Tray inside the obstacle, under the bridge (figure 9);
e) Tray inside the obstacle, on the bridge (figure 9).

Fig. 9 STARDUST: Different positions of the tray

Dust resuspended fraction is [6]:

$$\%R\_d = (D_{iw}-D_{fw})*100/D_{iw}$$

Where:

- %R_d = Percentage of dust resuspended.
- D_{fw}= Final Dust Weight;
- D_{iw} = Initial Dust Weight.

The weight of the dust has been measured by an electronic balance (precision 10^{-5} g).

All the experiments (except those with the tray under obstacle) were carried out also with the slit on the obstacle. Each set of experiments was repeated four times. Table 2 and Figure 10 shows the fraction of mobilized dust, obtained by the mean of the four experiments for each different experimental set-up.

			TUNGSTEN	*TEST*		
			1	***2***	***3***	***4***
		Tray Position	**No Obstacle (110°C)**	**Obstacle no Slit (110 °C)**	**Obstacle no Slit (25°C)**	**Obstacle with Slit (110°C)**
Mean mobilized fraction Valve B	***a***	***Bottom of the Tank***	16,6%			
	b	***Under Obstacle***		13,1 %	14,8 %	
	c	***Under Bridge***		0,8 %	0,1 %	0,3 %
	d	***Over bridge***		0,4 %	0,1 %	0,1 %
Mean mobilized fraction Valve A	***a***	***Bottom of the Tank***	0,2%			
	b	***Under Obstacle***		0,2 %	0 %	
	c	***Under Bridge***		0,1 %	0,1 %	0,2 %
	d	***Over bridge***		0,2 %	0,1 %	0,2 %

			STAINLESS STEEL 316	*TEST*		
			1	***2***	***3***	***4***
		Tray Position	**No Obstacle (110°C)**	**Obstacle no Slit (110 °C)**	**Obstacle no Slit (25°C)**	**Obstacle with Slit (110°C)**
Mean mobilized fraction Valve B	***a***	***Bottom of the Tank***	100 %			
	b	***Under Obstacle***		96,3 %	99,1 %	
	c	***Under Bridge***		0,5 %		0 %
	d	***Over bridge***		0,4 %	0 %	0 %
Mean mobilized fraction Valve A	***a***	***Bottom of the Tank***	0,1 %			
	b	***Under Obstacle***		0,1 %	0 %	
	c	***Under Bridge***		1,2 %		0 %
	d	***Over bridge***		0,3 %	0 %	0,1 %

			CARBON	*TEST*		
			1	***2***	***3***	***4***
		Tray Position	**No Obstacle (110°C)**	**Obstacle no Slit (110 °C)**	**Obstacle no Slit (25°C)**	**Obstacle with Slit (110°C)**
Mean mobilized fraction Valve B	***a***	***Bottom of the Tank***	100 %			
	b	***Under Obstacle***		96,8 %	98,4 %	
	c	***Under Bridge***		1,1 %		0,1 %
	d	***Over bridge***		0,7 %	0,2 %	0 %
Mean mobilized fraction Valve A	***a***	***Bottom of the Tank***	1,1 %			
	b	***Under Obstacle***		0,6 %	0,1 %	
	c	***Under Bridge***		1,0 %		0,1 %
	d	***Over bridge***		0,8 %	0,1 %	0,1 %

Table 2. Experimental results

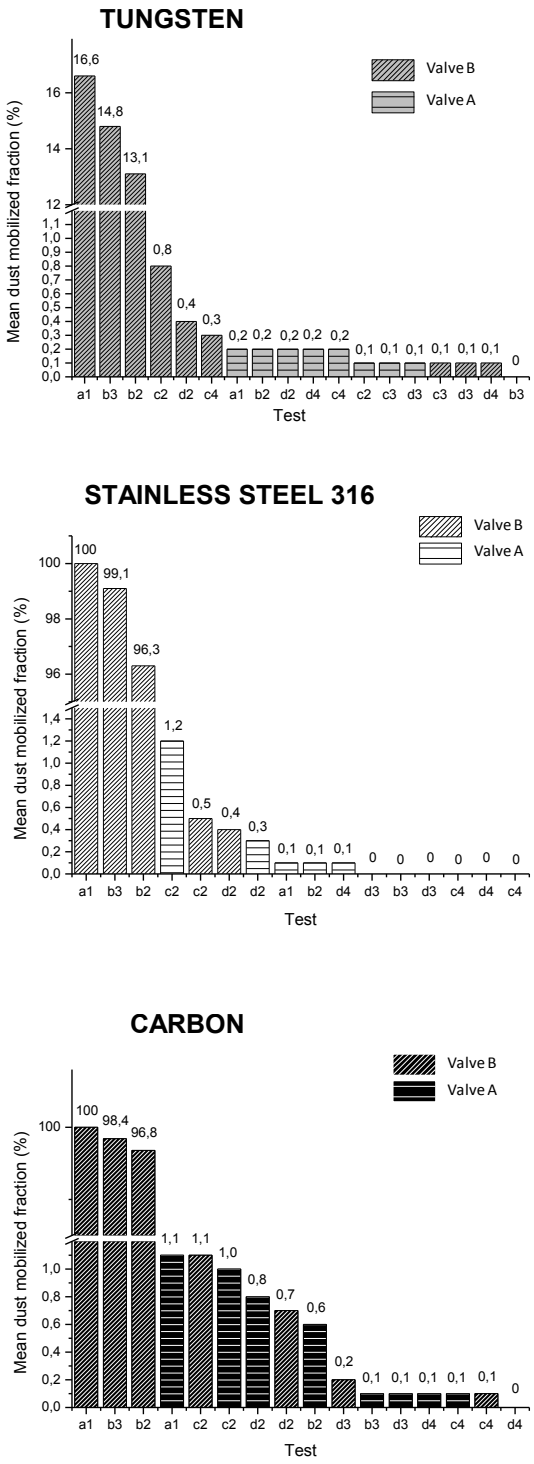

Figure 10. Mobilization fraction for each kind of dust per increasing amount of dust resuspended

Velocity measurements

In order to analyze the velocity magnitude inside STARDUST in case of LOVA a pressure transducer has been used. The pressure transducer used is a XCQ-093-2PSI Kulite instruments (Fig.11).

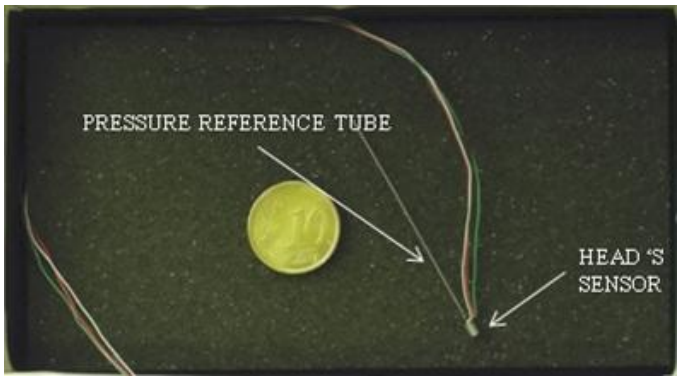

Fig. 11 Pressure transducer

It is a pressure detector realized with a monolithic piezo-resistive sensor in silicon that works in a temperature range from -60 to 125°C, although the pressure transducer operations are optimized for the temperature range from 25°C to 80°C. Its functioning is based on the piezo-resistive effect (that is the variation of electrical resistance due to the application of a mechanical force) generated on the silicon substrate by the pressure difference due to the air impact. The pressure transducer works with a 10 V DC alimentation in normal condition (but it can work with an alimentation up to 15 V) and it works in a differential mode. The pressure transducer output (in mV, with a maximum output value of 100 mV) is the value of the pressure difference between the dynamic pressure (measured by the head of the sensor) and the static pressure (measured by the pressure reference tube). The noise of the pressure reference tube is in the order of 2-3 mV (with maximum values of 5 mV)[10].
In order to measure the punctual velocity magnitude an ideal gas equation must be used [11]:

$$v = \sqrt{\frac{2\gamma R\overline{T}}{M(\gamma-1)}\left[\left(\frac{P_\Delta + P_s}{P_s}\right)^{\frac{\gamma-1}{\gamma}} - 1\right]}$$

where:

- γ : (c_p/c_v) (*~1.4* for air);
- R : universal gas constant [8,314 J/(mol*K)] ;
- $\overline{T}$: mean temperature ;
- M : air molecular mass (28,968 g/mol);
- P_s : static pressure ;
- P_Δ : differential pressure ($P_\Delta = P_T - P_s$).
- P_T : total pressure

The differential pressure (P_Δ) is automatically measured with the pressure transducer that gives the values obtained by the difference of total pressure (measured by the head of the sensor) and the static pressure (measured by the pressure reference tube) [11]. The static pressure is measured by a Pirani gauge (for a pressure rate between 100 Pa and 1000 Pa) and a Edwards gauge (for pressure rate from 1000 Pa to 95000 Pa) [11]. The temperature value is the mean value obtained by four thermocouples. The velocity data are stored at a frequency of 50 Hz [11].

The pressure transducer allows the punctual characterization of velocity flow field values [10]. During these experimental campaign the pressure transducer has been placed where dusts have been placed in the previous experiment:

- Tray without obstacle ;
- Tray under obstacle at the bottom part of the tank;
- Tray inside obstacle, under the bridge;
- Tray inside obstacle, over the bridge.

The experiments have been conducted only at 25°C in order to preserve the sensor integrity [12,13].

III. Experimental results

Quantitative measurements of dust resuspension
In this section the experimental results will be analyzed and discussed. In the following table (Tab.3) the acronyms to identify the experiments are shown:

1th Letter	W-C-SS	Dust's type (W:Tungsten, C:Carbon, SS : Stainless Steel)
2th Letter	A - B	Inlet position a : equatorial level b : divertor level
3th Letter	UO – UB – OB	Tray positions UO (Under Obstacle) : tray under obstacle UB (Under Bridge) : tray inside obstacle, under bridge OB (Over Bridge) : tray inside obstacle, on the bridge
4th Letter	h - c	Wall temperature h (hot) : wall heated up to 110 °C (operative conditions) c (cold) : wall at 25 °C (maintenance condition)
5th letter	s	Experiments done with a slit at bridge level to simulate the space between the limiter and the divertor inside ITER
Notes	NoObstacole	Experiments without obstacle

Tab. 3 Dust resuspension experimental setup acronyms

- Four test have been performed for each configuration;
- For each configuration the tray has been in order to take in account an imperfect tray cleaning;
- A 10% error was considered for each experiment in order to take in account the movements due to weighting operations.

Resuspended dust fraction has been calculated with a differential weighed:

$$\%R\_d = (D_{iw} - D_{fw})*100/D_{iw}$$

- %R_d = Percentage of dust resuspended.
- D_{fw} = Final Dust Weighted;
- D_{iw} = Initial Dust Weighted.

Fig.12 shows that the obstacle causes a reduction of mobilized dust for all the three types of dust. It is more sensitive (about 4%) in the case of SS and C at 110 °C, when the tray is placed under the obstacle. Another important aspect has to be taken in account is an increase of dust resuspended in case of cold experiments (at 25 °C) [14].

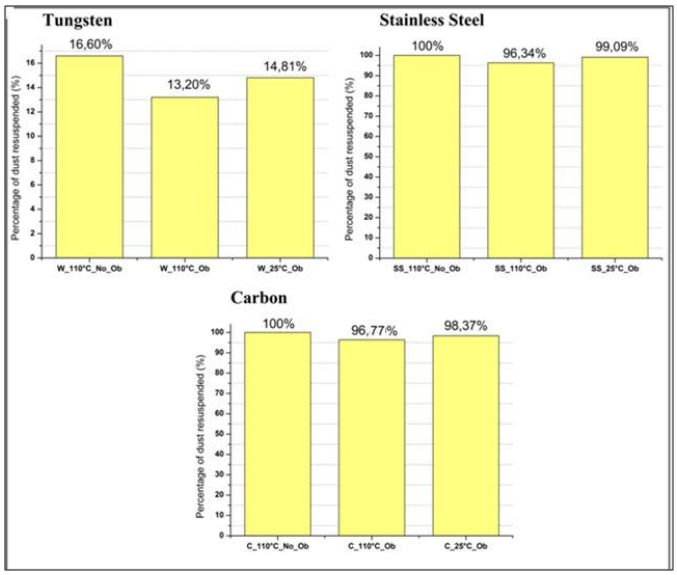

Fig.12 Tray in the bottom part of the tank, inlet B, Twall (110 °C and 25 °C), with and without obstacle

When the tray is placed inside the obstacle, and under the bridge (Fig.13) the quantity of mobilized dust is higher when the air inlet is at the divertor level (valve B). The slit seems to have a negative effect on dust mobilization. The local turbulence effect plays an important role in this reduction.

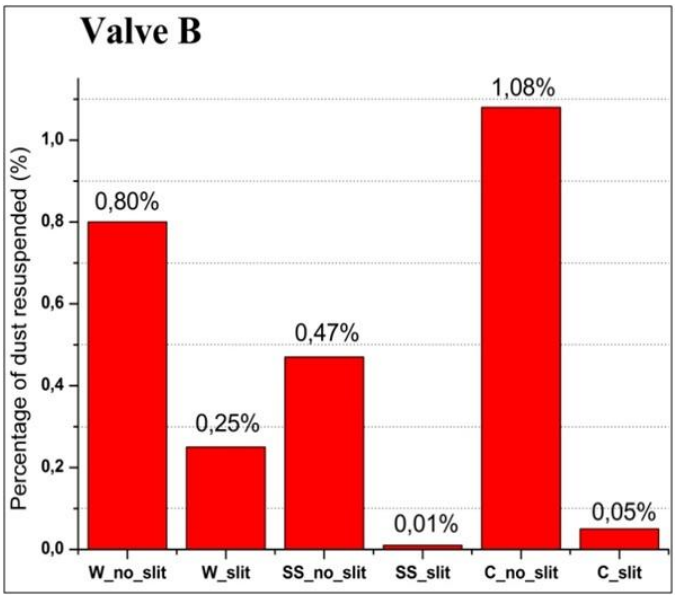

Fig.13 Slit effects on dust resuspension_Valve B experiments_Tray inside obstacle, under the bridge

For the experiments conducted with the tray inside the obstacle and under the bridge the quantity of mobilized dust is smaller (around 2% less) also with the slit on the obstacle and the air inlet is at the equatorial level (valve A). The comparison between the experiments at room temperature (walls at 25 °C) and hot conditions (walls at 110 °C) shows a higher mobilization for the cold tests. Fig.14 shows the test case in which the tray is placed inside the obstacle over the bridge and the air inlet is from the valve at the equatorial level (valve A).

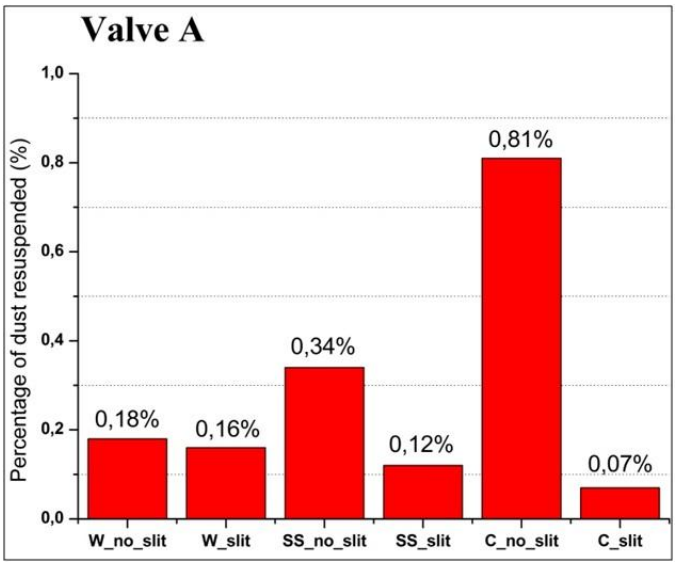

Fig.14 Slit effects on dust resuspension_Valve A experiments_Tray inside obstacle, over the bridge

Velocity measurements

Pressure transducer without obstacle and under obstacle, valve A

These experiments have been conducted by placing the tray with pressure transducer on the bottom part of tank without obstacle and under the obstacle both with inlet A. The comparison between maximum velocity values (and the parameters measured at maximum velocity values instant) is showed in Tab.4.

Exp	Time	Vel.	Internal Pressure	Vel. Error
	sec	m/s	Pa	%
A_UO_c	2	162,35	305,63	10,88
A_NoObstacle_c	2,88	214,21	311,19	13,80

Tab. 4 Maximum experimental velocity values for A_UO_c and A_NoObstacle_c

The velocity results show a maximum velocity reduction of almost 24% between the first configuration (A_UO_c) and the second one due to the screening effect of obstacle [15].

Pressure transducer without obstacle and under obstacle, valve B

These experiments have been conducted by placing the tray with pressure transducer in the bottom part of tank without obstacle and under obstacle both with inlet B. The results are shown in Tab. 5.

Exp	Time	Vel.	Internal Pressure	Vel. Error
	sec	m/s	Pa	%
B_UO_c	2,16	270,75	313,98	16,65
B_NoObstacle_c	1,48	296,29	122,84	17,70

Tab. 5 Maximum experimental velocity values for B_UO_c and B_NoObstacle_c

The velocity results show a maximum velocity reduction of 9% between the values measured in the first configuration (B_UO_c) and the second one (B_NoObstacle_c) due to the screening effect of obstacle [10,15].

Pressure inside obstacle, under the bridge, valve B, with and without slit

These experiments have been conducted by placing the tray with pressure transducer inside the obstacle, under the bridge and in the same position after the application of a slit with inlet B. The results are shown in Tab.6.

Exp	Time	Vel.	Internal Pressure	Vel. Error
	sec	m/s	Pa	%
B_UB_c_s	2	167,85	296,27	11,21
B_UB_c	2,5	179,63	436,63	11,90

Tab. 6 Maximum experimental velocity values for B_UB_c_s and B_UB_c

The velocity results show a maximum velocity reduction of almost 6,5 % between the values measured in the first configuration (B_UB_c_s) and the second one (B_UB_c) due to the turbulence effects of the slit that reduce velocity on the tray.[12,15]

Pressure inside obstacle, over bridge, valve A with and without slit

These experiments have been conducted by placing the tray with pressure transducer inside the obstacle, over the bridge and in the same position after the application of a slit at the bridge level that reproduce the space between limiter and divertor with inlet A. The results are shown in Tab.7.

Exp	Time	Vel.	Internal Pressure	Vel. Error
	sec	m/s	Pa	%
A_OB_c_s	2,5	176,71	473,76	11,74
A_OB_c	2,16	183,25	282,34	12,11

Tab. 7 Maximum experimental velocity values for A_OB_c_s and A_OB_c

The velocity results show a maximum velocity reduction of almost 3,5 % between the values measured in the first configuration (A_OB_c_s) and the second one (A_OB_c) due to the turbulence effects of the slit that reduce velocity on the tray.[12,15]

IV. NUMERICAL SIMULATIONS

Introduction

Due to the widespread and easily use of computer calculations, numerical models are fundamental tools for a great number of subjects under study. [16]. A two-dimensional (2D) modelling of STARDUST has been carried out. FLUENT, a commercially available CFD based on Finite Volume Method (FVM) solver together with the GAMBIT mesh generator, was used to simulate the flow behaviors for the same scenarios used during the laboratory tests. Finite Volume Method (FVM) was originally developed for fluid flow and heat and mass transfer calculations [17].

The results of these simulations were compared against the experimental data for CFD code validation. For validation purposes, the CFD simulation data were extracted at the same locations as the experimental data were collected.

Governing equations and thermodynamic models

Nomenclature

- *x, y, z* : coordinated axis
- p : static pressure (Pa)
- $\vec{v}$: velocity vector (m/s)
- u_i : component of velocity vector
- ρ : density
- S_m : is the mass added to the continuous phase from the dispersed second phase and any user-defined sources.
- μ : molecular viscosity (Pa·s)
- $\rho\vec{g}$: gravitational body force
- $\overrightarrow{F}$: external body force vector (N / m^3) that arise from interaction with the dispersed phase
- I : unit tensor
- $\bar{\bar{\tau}}_{eff}$: stress tensor.

The governing equations in a compressible turbulent flow can be written as follows in which gravity effects are included. The implemented fluid-dynamic model is based on the fully compressible formulation of the continuity equation and momentum equations:

$$\frac{\partial p}{\partial t}+\nabla\left(\rho v\right)=S_m$$

$$\frac{\partial}{\partial t}\left(\rho\vec{v}\right)+\nabla\cdot\left(\rho\vec{v}\vec{v}\right)=-\nabla p+\nabla\cdot\mu\left[\left(\nabla\vec{v}+\left(\nabla\vec{v}\right)^T\right)-\frac{2}{3}\nabla\cdot\vec{v}I\right]+\rho\vec{g}+\overrightarrow{F}$$

Turbulence is a main key for this kind of problems. The aim of this work is to get a preliminary overview of the fluid dynamics behavior of a LOVA event. The RNG-based $k-\varepsilon$ model has been chosen because its robustness. Also, the model chosen improves the accuracy for rapidly strained flows than the standard $k-\varepsilon$ model.

$$\frac{\partial}{\partial t}\left(\rho k\right)+\frac{\partial}{\partial x_i}\left(\rho k u_i\right)=\frac{\partial}{\partial x_j}\left(\alpha_k\mu_{eff}\frac{\partial k}{\partial x_j}\right)+G_k+G_b-\rho\varepsilon-Y_M+S_k$$

$$\frac{\partial}{\partial t}\left(\rho\varepsilon\right)+\frac{\partial}{\partial x_i}\left(\rho\varepsilon u_i\right)=\frac{\partial}{\partial x_j}\left(\alpha_\varepsilon\mu_{eff}\frac{\partial\varepsilon}{\partial x_j}\right)+C_{1\varepsilon}\frac{\varepsilon}{k}\left(G_k+C_{3\varepsilon}G_b\right)-C_{2\varepsilon}\rho\frac{\varepsilon^2}{k}-R_\varepsilon+S_\varepsilon$$

In these equations, G_k represents the generation of turbulence kinetic energy due to the mean velocity gradients, G_b is the generation of turbulence kinetic energy due to buoyancy, Y_m represents the contribution of the fluctuating dilatation in compressible turbulence to the overall dissipation rate. The quantities α_k and α_ε are the inverse effective Prandtl numbers for k and ε, respectively. S_k and S_ε are user-defined source terms. The model constants $C_{1\varepsilon}$, $C_{2\varepsilon}$ and $C_{3\varepsilon}$ have values derived analytically by the RNG theory. The RNG-based $k-\varepsilon$ turbulence model is derived from the instantaneous Navier-Stokes equations, using a mathematical technique called "renormalization group" (RNG) methods . The analytical derivation results in a model with constants different from those in the standard $k-\varepsilon$ model, and additional terms and functions in the transport equations for k and ε. The additional term in the ε equation given by:

$$R_\varepsilon=\frac{C_\mu\rho\eta^3\left(1-\eta/\eta_0\right)}{1+\beta\eta^3}\cdot\frac{\varepsilon^2}{k}$$

$$\eta\equiv S_k/\varepsilon;\eta_0=4.3;\beta=0.012$$

A more comprehensive description of RNG theory and its application to turbulence can be found in [18]. This model was developed to better handle low Re regions. In low flow regions, in the beginning of the LOVA event, the dissipation rate can become small and cause unrealistically high turbulent viscosities. RNG theory provides an analytically-derived differential formula for effective viscosity that accounts for low-Reynolds-number effects. The turbulent viscosity is calculated as:

$$d\left(\frac{\rho^2 k}{\sqrt{\varepsilon\mu}}\right)=\frac{1.72\hat{\nu}d\hat{\nu}}{\sqrt{\hat{\nu}^3-C_\nu}-1}$$

where μ is again the molecular viscosity, Cν is a constant, and $\hat{\nu}$ is the ratio of turbulent to molecular viscosity.

$$\hat{\nu}=\frac{\mu_t}{\mu},\quad C_\nu\approx100\quad \mu_t=\rho C_\mu\frac{k^2}{\varepsilon}$$

where C_μ is an empirical constant. Therefore, the turbulence will vary with the eddy scale. Effective use of this feature does, however, depend on an appropriate treatment of the near-wall region. Traditionally, there are two approaches to modeling the near-wall region. In one approach, the viscosity-affected inner region (viscous sublayer and buffer layer) is not resolved. Instead, semi-empirical formulas called "wall functions" are used to bridge the solution variables at the near-wall cells and the corresponding quantities on the wall, or in other therms the viscosity-affected region between the wall and the fully-turbulent region. In another approach, the turbulence models are modified to enable the viscosity-affected region to be resolved with a mesh all the way to the wall, including the viscous sublayer. This is called the "near-wall modeling" approach. In most high-Reynolds-number flows, the wall function approach substantially saves computational resources, because the viscosity-affected near-wall region, in which the solution variables change most rapidly, does not need to be resolved. The wall-function approach, however, is inadequate in situations where the low-

Reynolds-number effects are pervasive and the assumptions underlying the wall functions cease to be valid. Such situations require near-wall models that are valid in the viscosity-affected region and accordingly integrable all the way to the wall. In this case a enhanced wall treatment, with near wall refinement, has been chosen. Enhanced wall treatment is a near-wall modeling method that combines a two-layer model with enhanced wall functions. The two-layer approach is used to specify both ε and the turbulent viscosity in the near-wall cells. In this approach, the whole domain is subdivided into a viscosity-affected region and a fully-turbulent region. In the fully turbulent region the RNG-based $k-\varepsilon$ model is employed. In the viscosity-affected near-wall region the one-equation model of Wolfstein [19] is employed. The demarcation of the two regions is determined by a wall-distance-based, turbulent Reynolds number:

$$\mathrm{Re}_y \equiv \frac{\rho y \sqrt{k}}{\mu}$$

where y is the wall-normal distance calculated at the cell centers. The two-layer formulation for turbulent viscosity is used as a part of the enhanced wall treatment, in which the two-layer definition is smoothly blended with the high-Reynolds-number μ_t definition from the outer region, as proposed by Jongen [20]. To have a method that can extend its applicability throughout the near-wall region (i.e., viscous sub-layer, buffer region, and fully-turbulent outer region) it is necessary to formulate the law-of-the wall as a single wall law for the entire wall region. The code achieves this by blending the logarithmic (turbulent) laws-of-the-wall using a function suggested by Kader [21]. This approach allows the fully turbulent law to be easily modified and extended to take into account other effects such as pressure gradients or variable properties. The enhanced turbulent law-of-the-wall for compressible flow with heat transfer and pressure gradients has been derived by combining the approaches of White and Cristoph [22] and Huang et al. [23]. The production of turbulence kinetic energy, is computed using the velocity gradients that are consistent with the enhanced law-of-the-wall ensuring a formulation that is valid throughout the near-wall region.

The implemented CFD model solves the energy equation in the following form:

$$\frac{\partial}{\partial t}(\rho E) + \nabla \cdot \left(\vec{v}(\rho E + p) \right) = \nabla \cdot \left(k_{eff} \nabla T - \sum_j h_j \overrightarrow{J_j} + \left(\overline{\overline{\tau}}_{eff} \cdot \vec{v} \right) \right) + S_h$$

where k_{eff} is the effective conductivity, and $\overrightarrow{J_j}$ is the diffusion flux of species . The first three terms on the right hand side of equation represent energy transfer due to conduction, species diffusion, and viscous dissipation, respectively, includes the heat of chemical reaction, and any other volumetric heat sources. Heat transfer has been modelled using the Reynolds analogy, but for the RNG model, the effective thermal conductivity used in the energy equation is $k_{eff} = \alpha c_p \mu_{eff}$ where α (inverse of the turbulent Prandtl number) is calculated from Eq:

$$\left| \frac{\alpha - 1{,}3929}{\alpha_0 - 1{,}3929} \right|^{0{,}6231} \left| \frac{\alpha - 2{,}3929}{\alpha_0 - 2{,}3929} \right|^{0{,}3679} = \frac{\mu}{\mu_{eff}}$$

with $\alpha_0 = i / \mathrm{Pr} = k / \mu c_p$

Therefore, the turbulent Prandtl number is not constant as in the standard k–ε model, but it depends on the molecular Prandtl number. Developed analyses have been conducted in transitory regime with an real gas assumption according to the Aungier-Redlich-Kwong real gas model [24]. Thermo-physical properties of the air are assumed to be varying with the kinetic theory assumption.

Gas model

Some engineering problems involve fluids that do not behave as ideal gases. For example, at very high-pressure or very low-temperature conditions the flow cannot typically be modeled accurately using the ideal-gas assumption. Therefore, the real gas model allows to solve accurately for the fluid flow and heat transfer problems where the working fluid behavior deviate from the ideal-gas assumption. An equation of state is a thermodynamic equation, which provides a mathematical relationship between two or more state functions associated with the matter, such as its temperature, pressure, volume, or internal energy. One of the simplest equations of state for this purpose is the ideal gas law, which is roughly accurate for gases at low pressure gas region of the PT and PV diagrams. Ideal gas behavior can be expected when $P/P_c \ll 1$. Introduced in 1949, the Redlich-Kwong equation of state was a considerable improvement over other equations of that time. It is an analytic cubic equation of state and is still of interest primarily due to its relatively simple form. The original form is

$$P = \frac{RT}{V-b} - \frac{\alpha_0}{V(V+b)T_r^{0,5}}$$

- R= universal gas constant divided by molecular weight;
- V=specific volume;
- T=temperature;
- T_r=reduced temperature;
- α_0 e b are constants related directly to the fluid critical pressure and temperature.

ANSYS FLUENT has adopted the modified form from Aungier [25]. The Aungier-Redlich-Kwong equation has improved accuracy compared to the original form. This model employs a cubic equation of state of the following form [24] :

$$P = \frac{RT}{V-b+c} - \frac{\alpha(T)}{V(V+b)}$$
$$\alpha(T) = \alpha = \alpha_0 T_r^{-n}$$

$$c = \frac{RT_c}{P_c + \frac{\alpha_0}{V_c(V_c + b)}} + b - V_c$$

$$n = 0{,}4986 + 1{,}1735\omega + 0{,}4754\omega^2$$

$$\alpha_0 = 0{,}42747 R^2 T_c^2 / P_c$$

$$b = 0{,}08664 R\, T_c / P_c$$

$$R = \frac{R_u}{MW}$$

- P = absolute pressure (Pa);
- V = specific volume (m^3/kg);
- T = temperature (K);
- T_c = critical temperature (K);
- P_c = critical pressure (Pa);
- V_c = critical specific volume (m^3/kg);
- ω = acentric factor.

Enthalpy, entropy, and specific heat are computed in terms of the relevant ideal gas properties and the departure functions. The departure function F_{dep} of any conceptual property F is defined as [25] :

$$F_{dep} = F_{ideal}(T, P) - F(T, P)$$

where F_{ideal} is the value of the property as computed from the ideal gas relations. The departure function F_{dep} can be derived from basic thermodynamic relations and the equation of state. Following the above definition, the enthalpy H for the Aungier-Redlich-Kwong model is given by the following equations [26]:

$$H_{dep} = H_{ideal} - H_{dep}$$

$$H_{dep} = -PV + RT - \frac{1}{b}\left(T\frac{\partial \alpha}{\partial T} - \alpha\right) ln\left(\frac{V + b}{V}\right)$$

The specific heat c_p for the Aungier-Redlich-Kwong model can be derived by differentiating the equation for enthalpy with respect to T , and is given by:

$$c_p = c_{p,ideal} - c_{p,dep}$$

$$c_{p,dep} = -P\left(\frac{\partial V}{\partial T}\right)_p + R + \frac{d\alpha}{dT}\frac{(1+n)}{b} ln\left(\frac{V+b}{V}\right) - \alpha(1+n)\frac{\left(\frac{\partial V}{\partial T}\right)_p}{V(V+b)}$$

The entropy for the Aungier-Redlich-Kwong model is computed from the following equations

$$S = S_{ideal} - S_{dep}$$

$$S_{dep} = -Rln\left(\frac{V - b + c}{V_0}\right) - \frac{1}{b}\frac{d\alpha}{dT} ln\left(\frac{V+b}{V}\right)$$

Pre-processing

The geometry of the computational model has been created using Gambit software. For the discretization of the overall domain, 59056 quadrilateral cells have been adopted. An important feature when discretising the computational domain is to have a sufficient refinement along the direction of velocity gradient, namely normal at the inlet section in our case. The characteristics of the grid used in simulations is listed in Tab. 8. and a grid sketch is presented in Fig.15.

Initial Mesh	
Cells	59056
Faces	120783
Nodes	61727
Maximum cell squish	0,296055
Maximum aspect ratio	4,38624

Tab.8 : Mesh characteristics

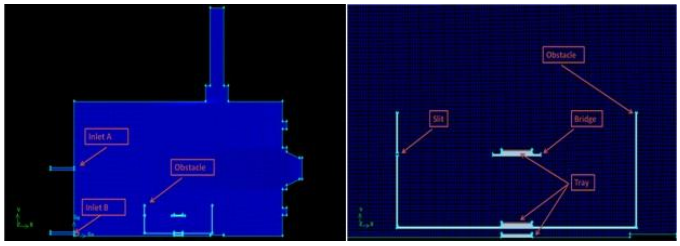

Fig.15 Grid sketch

Grid independence is an important stage in CFD modeling. Grid independence was achieved by using a solution adaptive refinement, as cells can be added where they are needed in the mesh. The initial grid was adapted by putting more cells in the areas where the density gradient is higher than a chosen level. This process was repeated until the results became grid independent. Fig.16 shows three 2D meshes: Mesh at 0.5s of 48649 cells, Mesh at 2s of 55432 cells, and Mesh at 4s of 219709 cells.

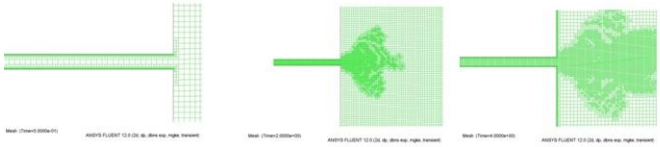

Fig.16 Mesh 2D with adaptation

The last one shown above supplied reasonable performances in terms of CPU time. A mesh boundary layer was also considered on the wall of the model so that the mesh density can be increased to sufficiently resolve the boundary layer, without substantially increasing the total number of nodes. The boundary layer has been created dynamically by wall-refinement in order to improve the performance of the mesh. The wall-refinement consists of thinner cells in the vicinity of the wall, ranging from 0,1875mm thick (attached to the wall) growing up to 3mm . The resulting grid is shown in Fig.17.

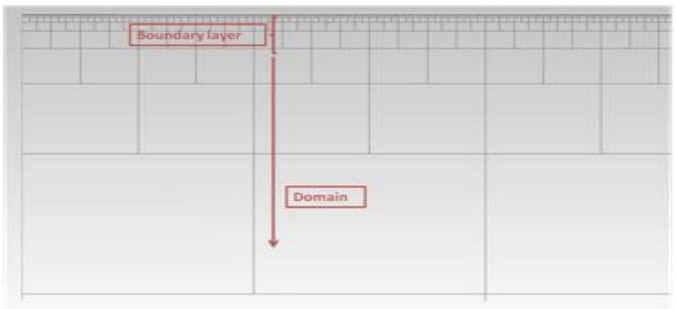

Fig.17 Boundary layer

The basic parameters of the simulation are showed in Tab.9 :

Representative System Parameters	
Molar mass (Air) [kg/kmol]	28,966
Inlet Temperature [K]	292,75
Inlet Pressure [Pa]	280000
Internal Temperature [K]	292,16767
Internal Pressure [Pa]	99,16735
Wall temperature [K]	300,15
Wall temperature (Heated Wall) [K]	383,15

Tab.9 Representative System Parameters

In the $k-\varepsilon$ based model, we need to specify the turbulence length scale as well as turbulence intensity. Typical value of turbulence intensity is chosen to be between 5% and 10%. There is no noticeable difference in the results if turbulence intensity is varied in the range as showed in Tab.10.

Turbulence Parameter (k-ε RNG)	
Turbulence Intensity	5%
Turbulence Length Scale [mm]	0,63

Tab.10 Turbulence parameters

A commonly used set-up of boundary conditions was configured. The gas inlet was taken as a experimental mass-flow inlet with a inlet function given in Fig. 18 in order to take into account the time necessary for the opening of the inlet valve and the time necessary to reach the regime of the mass flow rate. All the other surfaces are treated as adiabatic walls with a no-slip boundary condition.

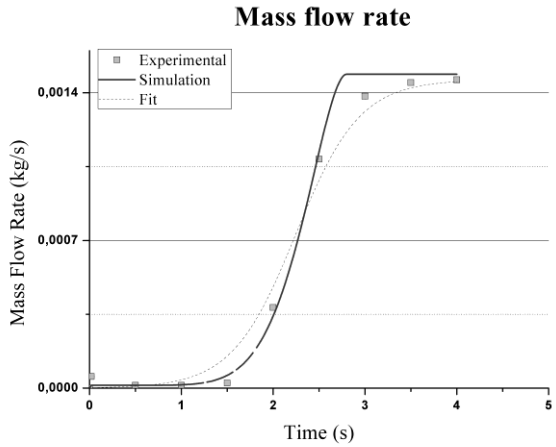

Fig.18 Flow rate function (experimental and simulated)[20]

For the 110°C and 25°C tests temperature conditions are set at the lateral walls.

Numerical schemes and parameters

Simulations have been carried out with the 2D, with a virtual third dimension, density-based solver in a unsteady formulation available in FLUENT. A second order Third-Order MUSCL discretization scheme has been used for momentum, turbulent kinetic energy, turbulent dissipation rate, and energy. Gradients are estimated by the Green-Gauss node based method. The solution process is iterative and a convergence criterion is required. Convergence was assumed for each time step as all residuals fall below 10−3, and a maximum of 200 iterations per time step was considered if the residuals failed to pass these thresholds (Fig.19).

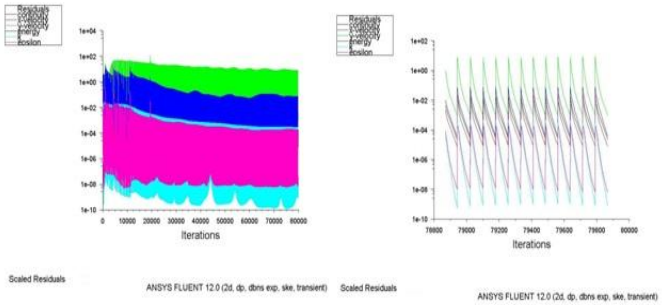

Fig.19 Residuals

While time steps of 0.02s would have been sufficient in order to account the transient and compare the simulation with the experimental data, convergence concerns implied to use a time step no greater than 1e-5s in all simulations.

V. Numerical Results-Simulation with and without Obstacle

The actual computation time taken for solving a 4 seconds transient, using 2D turbulent model with enhanced wall treatment, is 72 h. The computations were performed using the CFD software on a AMD Phenom 9600 Quad Core with 8 GB of memory and a maximum speed of 2,26 GHz. Fig.20 shows the vacuum breakdown:

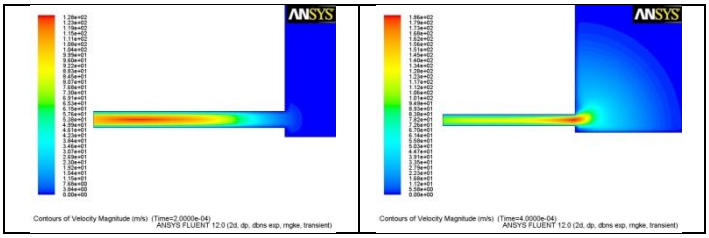

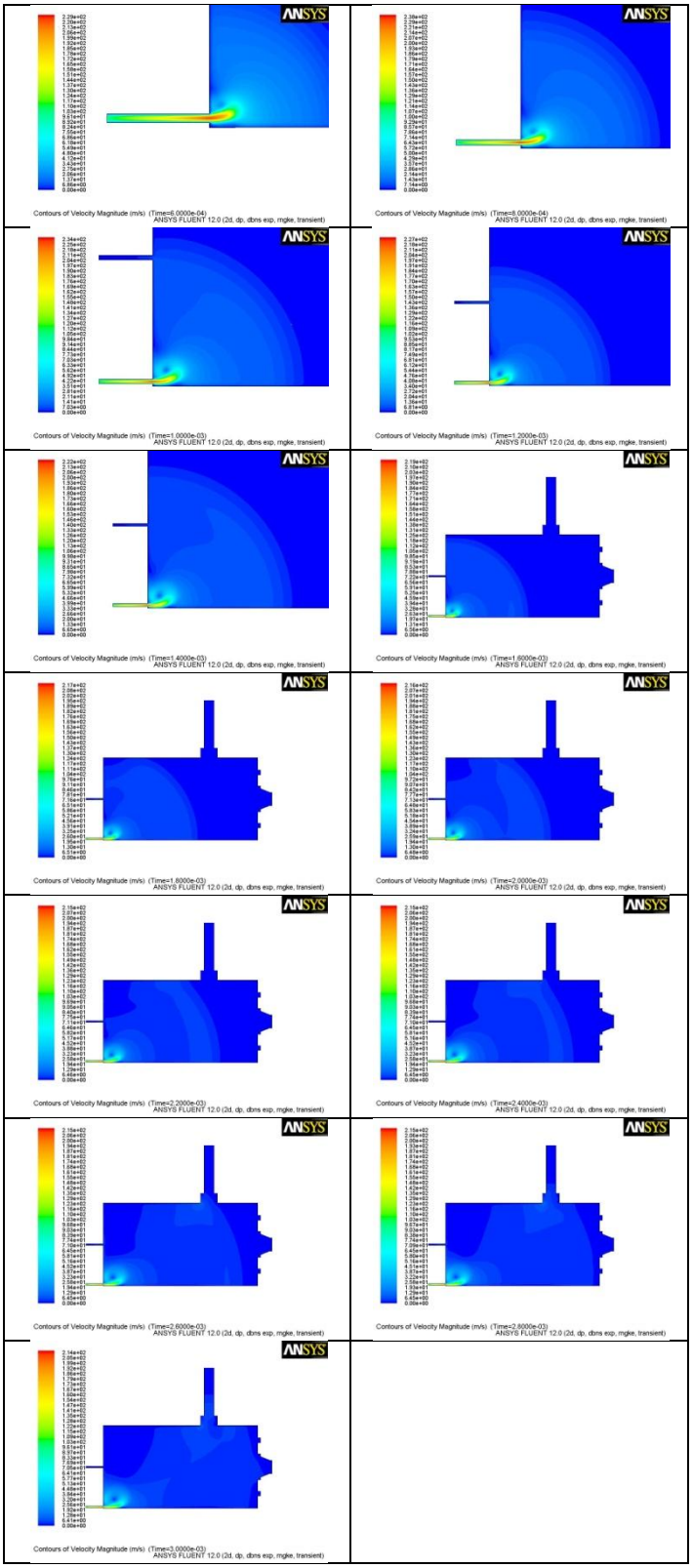

Fig. 20. Vacuum breakdown

This initial phase is too fast to be recorded with the velocity experimental set-up used for this experimental (sample rate 50Hz) campaign.

Fig.21 illustrates the velocity magnitude in the whole domain at the end of simulation when the flow is totally expanded:

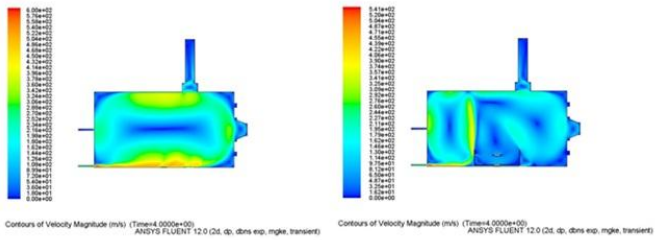

Fig.21 Velocity magnitude

The maximum velocity was about 600m/s. At the end of the inlet tube an expanding airflow with Mach Number M = 3÷3.66 (for the different tests) was realized. Future works will be focused on hypersonic flow interaction with obstacle [27] and local temperature measure with optical method.

In the following table (Tab.11) the velocity magnitude values at 2s in different experimental configuration are showed.

It was shown that dust mobilization fraction may change from 100%, if an air stream that enters the vacuum vessel directly hits the dust sample, to well below 1%, if the air stream is entering far from the dust location. The velocity results in table 11 can support the mobilization rate only for the experiments without obstacle. In fact in this case the difference in the velocity between air inlet from valve A and valve B (from 150-188 m/s to 385-413 m/s) are consistent with the mobilization from 1% in the first case to 100% in the second one. The velocity curves relating to the cases in which the obstacle is inside the tank are showed in figure 22. It is evident that the differences in the velocity values between air inlet from valve A and valve B do not justify the differences in the mobilization.

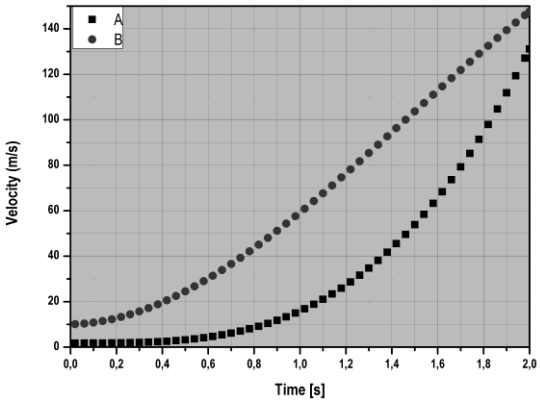

Fig. 22. Numerical velocity values under obstacle, valve A and valve B

	Tray Position	No Obstacle (25C)	Obstacle no Slit (25C)	Obstacle and Slit (25C)	No Obstacle (110C)	Obstacle no Slit (110C)	**Obstacle and Slit (110C)**
Velocity Magnitude Inlet Valve A [m/s]	Over bridge		69,259	68,554		90,116	89,240
	Under Bridge		32,84	32,92		44,79	44,90
	Under Obstacle	See Bottom of the Tank	131,183	131,709	See Bottom of the Tank	163,342	163,99
	Bottom of the Tank	150,868			187,853		
Velocity Magnitude Inlet Valve B [m/s]	Over bridge		30,124	29,561		39,214	38,481
	Under Bridge		59,279	59,122		86,221	73,616
	Under Obstacle	See Bottom of the Tank	147,599	147,807	See Bottom of the Tank	201,284	201,568
	Bottom of the Tank	384,997	-	-	413,573	-	-

Tab.11 Velocity magnitude at 2s for different positions

These results suggest that the nodelization of the zone under the obstacle needs additional refinement, to fit better the mobilization data. The experimental data of the velocity taken in this critical zone are the key point to resolve this issue.

Figure 23. shows the temperature field, for both 110°C and 25°C test.

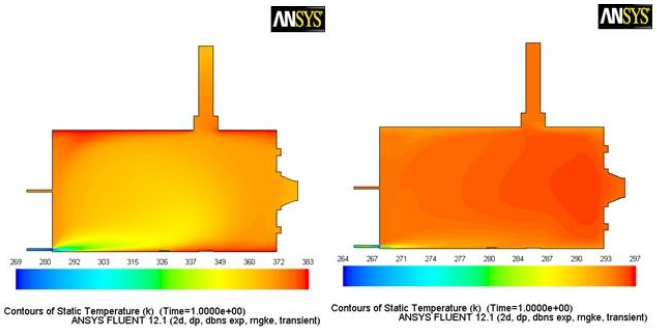

Figure 23. Temperature field for hot (left) wall and cold (right) transient

In the present study, our concerns are primarily focused on modeling the turbulent flows; detailed dispersion and deposition patterns particles are not studied. However we tried to simulate particle paths only as a crude prediction of the dispersion of particles under turbulence. We cannot yet solve for the particle trajectories with a density based solver and a real gas model, so we look at massless particle paths in the flow. This assumption, namely particles will follow the fluid streamlines closely, is true only for Carbon and Tungsten because of the Stokes number was evaluated at the inlet section flow conditions (table 12).

Stokes Numbers			
	SS316	Carbon	Tungsten
Mean particle diameter [μm]	25	4,5	0,4
Particle density [kg/m^3]	8000	2267	19250
Stokes number	23,68	0,21	0,016

Table 12. Stokes Numbers

These tracer particles are released from the inlet because the constrains of the software usable by the numerical solver. The particle paths are shown in figure 24.

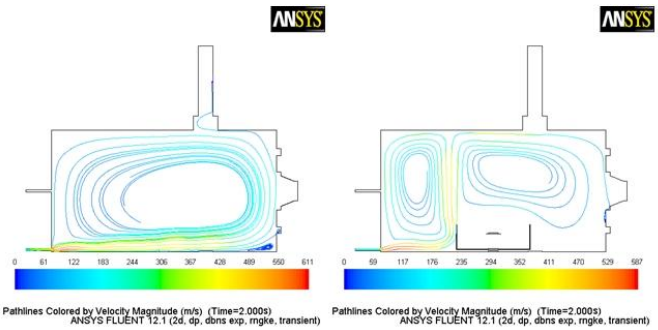

Figure 24. Pathlines of the particles without (left) and with (right) obstacle

Although the flow pattern is very important in determining the dispersion and deposition of particles, the particle motion would naturally depend on physical characteristics of the dust, such as their physical dimensions, electric and hygroscopic properties.

Static pressure output

The models used for the simulation were:

- Real gas based Standard k-ε;
- Ideal gas based k-ε;
- RNG-based k-ε turbulence.

Each pressure static trend obtained by the different models has been compared with the experimental one is shown in Fig.25:

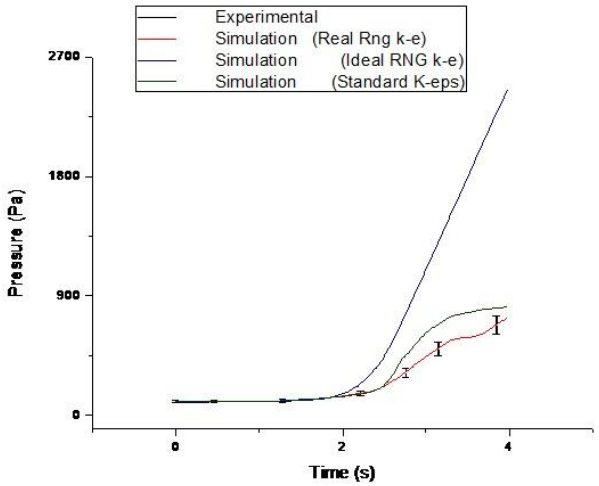

Fig.25 Pressurization rate (experimental and simulated)[15]

It can be seen that the coupling of real gas assumption and RNG-based k-ε turbulence model could be used to simulate the LOVA event better than the real gas based Standard k-ε and the ideal gas based k-ε because the numerical pressure static numerical results match with the experimental ones better than the other models.

VI. Numerical and Experimental Data Comparison

A simulated low pressurization rate (300 Pa/s) LOVA event in ITER like, due to a small air leakage for two different

positions of the leak, at the equatorial port level and at the divertor port level, has been carried out in order to evaluate the influence of obstacles, such as the divertor and the LDG, and temperature on dust resuspension during both maintenance and operative conditions. To keep into account the ITER VV wall conditions of temperatures found during operations, the external walls of STARDUST were heated up to 110°C. In another set of experiments the temperature was set to 25°C, which represents the condition during maintenance operations. All the experimental conditions have been simulated to analyze the thermo-fluid dynamics behavior inside STARDUST in case of a LOVA. In this section it will be discussed the correspondence between the variation of velocity magnitude, provided by the simulations and experiments with pressure transducer, and the relative dust mobilization for different characteristic points, in order to better understand how different ITER VV conditions may influence the mobilization of the dust in case of a LOVA. The correspondence is guaranteed by the Stokes Number only for Tungsten and Carbon.

Obstacle influence in dust mobilization

The experimental results obtained at an assigned temperature, for both the valve A and the valve B, show a reduction of dust resuspended when the tray is placed under the obstacle. Hence it is possible to state that the divertor causes the diminution of mobilized dust for W and C for a leakage from both the equatorial and the divertor port level. In case of a leakage at the divertor port level the influence of the obstacle is bigger than at the equatorial one. The effect of the presence of the obstacle on the mobilization, i.e. the reduction of the resuspension due to the divertor, is shown in Fig. 26 for the valve A and the valve B. All the variations of the velocity magnitude and the mobilization shown in this section refer to the configuration with the tray under the obstacle (Tab.13).

Divertor effect (valve A)			
	Without obstacle	*With obstacle*	*Variation between the configurations (%)*
Tungsten (mobilization %)	0,20	0,20	**0,00**
Carbon (mobilization %)	1,10	0,60	**-0,50**
Simulation velocity (m/s)(at 2 sec)	187,85	163,34	**-13,048**
Experimental velocity (m/s)	214,21	162,35	**-24,210**
Divertor effect (valve B)			
	Without obstacle	*With obstacle*	*Variation between the configurations (%)*
Tungsten (mobilization %)	16,60	13,10	**-3,50**
Carbon (mobilization %)	100,00	98,40	**-1,60**
Simulation velocity (m/s)(at 2 sec)	413,47	201,28	**-51,319**
Experimental velocity (m/s)	296,29	270,754	**-8,619**

Tab.13 Percentage variation due to the obstacle

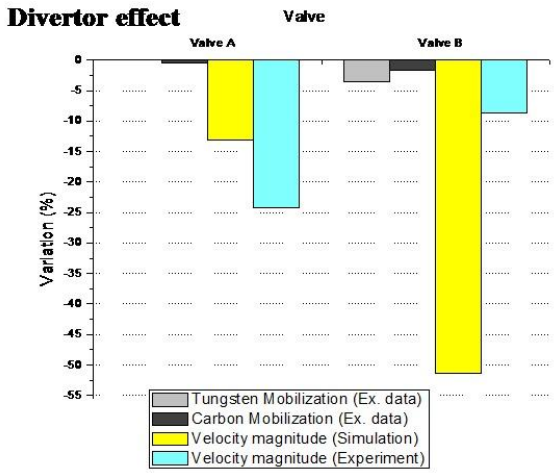

Fig.26 Effect of the divertor: comparison between experimental dust mobilization and velocity magnitude

For both dusts used and for both valves there is a reduction of the mobilization related to the reduction of the velocity magnitude. The previous graph also shows the bigger influence of the divertor on the mobilization and the velocity, when a LOVA occurs from divertor port level.

Temperature influence in dust mobilization

The experimental results obtained at different temperatures (raising from 25°C, during maintenance conditions, to 110°C, operative conditions) show for the valve B (the higher dust mobilization experimental configuration) a reduction of dust resuspended when the temperature increases despite of a higher velocity magnitude obtained by the numerical analysis. The effect of the temperature is shown in Fig. 27 for valve B. All the variations of the velocity magnitude and the mobilization shown in this section refer to the configuration with the tray under the obstacle (Tab.14).

Temperature effects (valve B)			
	Hot condition	*Cold condition*	*Variation between the configurations (%)*
Tungsten (mobilization %)	13,2	14,81	**-1,61**
Carbon (mobilization %)	96,8	98,37	**-1,57**
Simulation velocity (m/s)(at 2 sec)	201,28	147,60	**26,67**

Tab.14 Percentage variation between cold and hot wall's condition

In case of a LOVA occurring during operative conditions, the mobilization is lesser than the maintenance conditions one. The result of the numerical analysis seems to be in contrast with the experimental evidences. It can be explained with the higher relative humidity value at lower temperature that may influence the dust agglomeration properties, causing the increase of the air-dust impact surface.

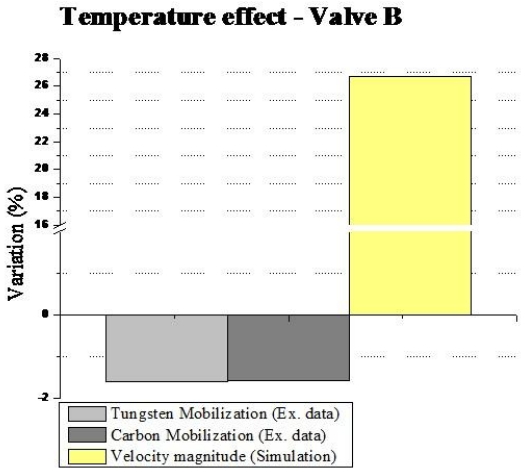

Fig.27 Effect of the increase of the temperature (from Twall = 25°C to Twall = 110°C): comparison between dust mobilization and simulated velocity magnitude

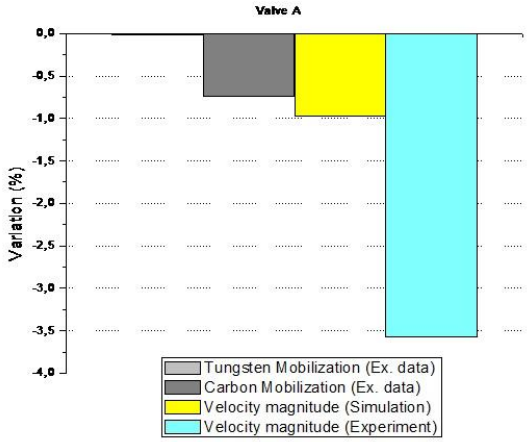

Fig.28 Effect of the slit: comparison between experimental dust mobilization and simulated and experimental velocity magnitude – Valve A

Slit influence in dust mobilization

The experimental results obtained at a assigned temperature, show a reduction of dust resuspended in case the tray is placed over the bridge (inlet from the valve A) and under the bridge (inlet from the valve B) if a slit is applied on the obstacle at the bridge level (Tab.15). The effect of the slit is shown in Fig.28 and Fig.29.

SLIT EFFECT (Valve A)			
	Without slit	*With slit*	*Variation between the configurations (%)*
Tungsten (mobilization %)	0,20	0,18	**-0,02**
Carbon (mobilization %)	0,81	0,07	**-0,74**
Simulation velocity (m/s)(at 2 sec)	90,11	89,24	**-0,971**
Experimental velocity (m/s)	183,25	176,71	**-3,569**
SLIT EFFECT (ValveB)			
	Without slit	*With slit*	*Variation between the configurations (%)*
Tungsten (mobilization %)	0,80	0,25	**-0,55**
Carbon (mobilization %)	1,08	0,05	**-1,03**
Simulation velocity (m/s)(at 2 sec)	86,22	73,62	**-14,619**
Experimental velocity (m/s)	179,63	167,85	**-6,555**

Tab.15 Slit influence

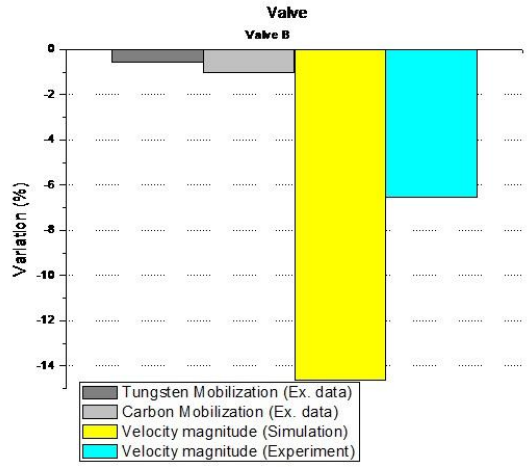

Fig.29 Effect of the slit: comparison between experimental dust mobilization and simulated and experimental velocity magnitude – Valve B

The limiter-divertor gap seems to have a negative effect on the dust mobilization. The local turbulence effect appears to play an important role in this reduction as shown in numerical results.

VII. Conclusion

By means of STARDUST facility a simulated low pressurization rate (300 Pa/s) LOVA event in ITER due to a small air leakage for two different positions of the leak has been carried out in order to evaluate the influence of obstacles and different temperature conditions on dust resuspension. For the experiments done with the dust inside the tank (with and without obstacle) the most important evidences were:

- The obstacle causes a diminution of mobilized dust for all the three types of dust. It is more sensitive (about 4%) in the case of SS and C at 110 °C, when the tray is placed under the obstacle.

- When the tray is placed inside the obstacle and under the bridge the quantity of mobilized dust is up to 3% maximum when the air inlet is at the divertor level (valve B). The slit seems to have a negative effect on the dust mobilization. From the experiments conducted with the tray inside the obstacle and in both configuration (under and over the bridge, Valve A) the quantity of mobilized dust is smaller also in the case when there is the slit on the obstacle. The local turbulence effect plays an important role in this reduction;
- Another important aspect that has to be taken into account is an increase of dust resuspended in case of cold experiments (at 25 °C), made to simulate a LOVA during maintenance conditions.

By placing the pressure transducer in the same position of the tray (in maintenance conditions) the variation of the velocity measured in different experimental configurations is in accordance with the dust mobilization which means that the previous considerations are correct. A two-dimensional (2D) modeling of STARDUST has been carried out. For validation purposes (the correspondence between dust and flow lines is guaranteed by the Stokes Number only for Tungsten and Carbon), the CFD simulation data were extracted at the same locations as the experimental data were collected. The velocity variations of the numerical simulation are in accordance with the velocity experimental variations and the dust resuspended variations [except for the case of the tray under the obstacle], valve B, at different temperatures (raising from 25°C to 110°C) that show a reduction of dust resuspended when the temperature increases despite of a higher velocity magnitude obtained by the numerical analysis. The result of the numerical analysis seems to be in contrast with the experimental evidences. It can be explained with the higher relative humidity value at lower temperature that may influence the dust agglomeration properties, causing the increase of the air-dust impact surface. It is possible to conclude by saying that:

- For both dusts used and for both valves there is a reduction of the mobilization related to the reduction of the velocity magnitude. The previous graph also shows the bigger influence of the divertor on the mobilization and the velocity, when a LOVA occurs from divertor port level ;
- In case of a LOVA occurring in operative conditions, the mobilization is lesser than the maintenance conditions one;
- The limiter-divertor gap seems to have a negative effect on the dust mobilization. The local turbulence effect appears to play an important role in this reduction.

ACKNOWLEDGMENT

We would like to thank the personnel of Dipartimento di Ingegneria Meccanica of "Tor Vergata" University for their support. We know we have found a lot of new friends during this season. Special thanks to Riccardo Quaranta, fundamental one to conclude this task and special friend. I would like to thank the complete staff of the Dottorato di Ricerca di Elettronica Quantistica e Plasmi. They were fantastic and very patient to attend and help solving our several requests. Special thanks to Professor Carlo Bellecci, Professor Sergio Martellucci, Dr.Maria Richetta, Dr.Michela Gelfusa, Renato Marchetti and Eugenio Penco for all the support. We would like to thank our colleagues of the ENEA Frascati, specials thanks to Dr.Maria Teresa Porfiri and Rodolfo Borelli. We would like to thank also our colleagues of the Joint European Torus.

REFERENCES

[1] Benchawan Wiwatanapataphee, Kittisak Chayantrakom, and Yong-Hong Wu , "Mathematical Modelling and Numerical Simulation of Fluid-Magnetic Particle Flow in a Small Vessel", INTERNATIONAL JOURNAL OF MATHEMATICAL MODELS AND METHODS IN APPLIED SCIENCES-35.pdf.

[2] J.P. Sharpe, D.A. Petti, H.-W. Bartels, *A review of dust in fusion devices: implications for safety and operational performance*, Fusion Eng. Des. 63–64 (2002) 153–163.

[3] J.Winter, *Dust: a new challenge in nuclear fusion research*, Phys. Plasmas 7 (2000) 3862–3866.

[4] J.P. Sharpe, P.W. Humrickhouse, *Dust mobilization studies in the TDMX facility*, Fusion Engineering and Design 81 (2006) 1409–1415.

[5] E. Eberta, J. Raeder, *LOCA, LOFA and LOVA analyses pertaining to NET/ITER safety design guidance*, Fusion Engineering and Design 17, (1991) Pages 307-312.

[6] ITER-JCT Generic Site Safety Report N84 Garching (Germany), July 2001

[7] C.Bellecci, P.Gaudio, I.Lupelli, A.Malizia, M.T.Porfiri, R.Quaranta, M. Richetta. *"Charaterization of divertor influence in case of LOVA: Analysis stardust facility and thermofluidodynamics simulation"*, EPS2009 Proceedings, 36th EPS Conference on Plasma Phys. Sofia-Bulgaria, 29 June-3 July 2009, ECA Vol.33E, P1.086.

[8] M.T. Porfiri, N. Forgione, S. Paci, A. Rufoloni, Dust mobilization experiments in the context of the fusion plants—STARDUST facility, Fusion Engineering and Design 81 (2006) 1353–1358.

[9] M. T. Porfiri, S. Libera, S. Paci, A. Rufoloni, L. Verdini, STARDUST facility : first series of the tungsten dust mobilization experiments, FUS-TN-SA-SE-R-94, 2003.

[10] Kulite Technical chart for Pressure Transducer XCQ-093-2PSI-D

[11] A.Kurtz, J. VanDWeert, B.Kochman, *"Pitot-Static Transducer"*, Kulite Semiconductor Product, Inc

[12] C. Bellecci, P. Gaudio, I.Lupelli, A.Malizia, M.T.Porfiri, M. Richetta. Misure di mobilizzazione e trasporto nella facility STARDUST, Società Italiana di Fisica , XCIV Congresso Nazionale, Genova 22-27 Settembre 2008, Lunedì 22 Settembre Sezione V – Fisica Applicata (2008).

[13] C.Bellecci, P.Gaudio, I.Lupelli, A.Malizia, M.T.Porfiri, R.Quaranta, M. Richetta. "Charaterization of divertor influence in case of LOVA: Analysis stardust facility and thermofluidodynamics simulation", EPS2009 Proceedings, 36th EPS Conference on Plasma Phys. Sofia-Bulgaria, 29 June-3 July 2009, ECA Vol.33E, P1.086.

[14] C. Bellecci, P. Gaudio, I. Lupelli, A. Malizia, M.T. Porfiri, M. Richetta. Dust mobilization and transport measures in the STARDUST facility, EPS2008 Proceedings, 35th EPS Conference on Plasma Phys. Hersonissos, 9 - 13 June 2008 ECA Vol.32, P-1.175 (2008).

[15] C.Bellecci, P.Gaudio, I.Lupelli, A.Malizia, M.T.Porfiri, R.Quaranta, M. Richetta. "Velocity flow field characterization inside stardust experimental facility: comparison between experimental campaign and numerical simulation results", ICENES2009 Proceedings, 14th International Conference on Emerging Nuclear Energy Systems. Ericeira-Portugal, 29 June – 3 July, ICENES Proceedings.

[16] Marius-Constantin O.S. Popescu, Nikos E. Mastorakis, Cornelia A. Bulucea, Liliana N. Perescu-Popescu, "Electromagnetic and Thermal Model Parameters", INTERNATIONAL JOURNAL OF ENERGY, Issue 4, Vol. 2, 2008

[17] S.R. Sabbagh-Yazdi, M.T. Alkhamis, M. Esmaili and N.E. Mastorakis], " Finite volume analysis of two-dimensional strain in a thick pipe with internal fluid pressure", INTERNATIONAL JOURNAL OF MATHEMATICAL MODELS AND METHODS IN APPLIED SCIENCES-75.pdf

[18] S.A. Orszag, V. Yakhot, W.S. Flannery, F. Boysan, D. Choudhury, J. Maruzewski, and B. Patel, Renormalization Group Modeling and Turbulence Simulations, International Conference on Near-Wall Turbulent Flows, Tempe Arizona (1993).
[19]] M. Wolfstein, The Velocity and Temperature Distribution of One-Dimensional Flow with Turbulence Augmentation and Pressure Gradient, Int. J. Heat Mass Transfer, 12:301-318, 1969.
[20] T. Jongen, Simulation and Modeling of Turbulent Incompressible Flows, PhD thesis, EPF Lausanne, Lausanne, Switzerland, 1992.
[21] B. Kader, Temperature and Concentration Profiles in Fully Turbulent Boundary Layers, Int. J. Heat Mass Transfer, 24(9):1541-1544, 1981.
[22] F. White and G. Christoph, A Simple New Analysis of Compressible Turbulent Skin Friction Under Arbitrary Conditions, Technical Report AFFDL-TR-70-133, February 1971.
[23] P. Huang, P. Bradshaw, and T. Coakley, Skin Friction and Velocity Profile Family for Compressible Turbulent Boundary Layers, AIAA Journal, 31(9):1600-1604, September 1993.
[24] R. W. Johnson, The handbook of fluid dynamics, Cambridge University Press (1998).
[25] R. H. Aungier. A Fast, Accurate Real Gas Equation of State for Fluid Dynamic Analysis Applications. Journal of Fluids Engineering, 117:277-281, 1995.
[26] B.E. Poling, J.M. Prausnitz, and J.P. O Connell. The properties of Gases and Liquids. McGraw-Hill, International Edition, 5th edition, 2007.
[27] Salimuddin Zahir and Zhengyin Ye , " Hypersonic Flow Interaction of Pitched Plates on Blunted Cone at Incidence", INTERNATIONAL JOURNAL OF MATHEMATICAL MODELS AND METHODS IN APPLIED SCIENCES-22.pdf.

P.Gaudio

From 1994 to 1995
Research job started with an international collaboration in LITE (LIDAR In-Space Technology Experiment 10-19 September 1994) mission. During this period, in joint with the LITE mission, he was involved in an intensive Lidar Measurements campaign in Potenza and Napoli. As INFM student he worked for two years on absorption coefficient problems. During these years he projected and developed an absorption cell to study the interaction of a laser beam with samples of pollutants gases. He collected a wide absorption data base on several pollutants gases as: Freon 11, Freon 12, Methane, Ethylene, etc.
From 1996 to July 1998
INFM (National Institute on the Phisic Matter now CNR) Researcher. He was involved in project, development and improvement of a ground based CO2 Lidar/Dial system. He made several measurements campaign to study water vapour and ozono cycle and Planetary Boundary Layer (PBL) height measurements
From July 1998 to March 2000
CRATI s.c.r.l. Researcher. In this period, in collaboration with the Quantum Electronic and Plasma Laboratory of the University of Rome "Tor Vergata", he worked to the project and development of a mobile Lidar/Dial setup. He made several measurements campaigns to test the mobile system and to study diffusion into the atmosphere of a plume emitted from factory chimneys. In this period he studied the possibility to inject a CW CO2 Laser into a TE laser at the aim of future Lidar doppler applications.
From March 2000-2006
Research technician at University of Rome "Tor Vergata". He worked to develop and improve a Lidar/Dial setup and he is involved in the measurements of water vapour cycle and columnar atmospheric contents. He studies aerosol plume emitted by forest fire and its interaction with laser beams. He also studies how to improve the performances of laser sources adopted for Lidar/Dial applications. He studied the possibility to use the Lidar/Dial systems to detect forest fire and reduce the false alarm. At this aim he projected a compact mobile Lidar Dial setup. He begins to work in the field of laser plasma interaction system. He developed a laser plasma system based on a gas supersonic jet of Xenon as target. He utilizes these devices allow relevant applications in microscopy analysis since they permit to obtain images of flash of life of the tested biological sample. A scientific collaboration with the ENEA Frascati- Fusion Department is started. The aim of this collaboration is studying the dust mobilization problem inside the nuclear fusion reactors. In this line he is studying the possibility to measure the evolution of the dusts, in case of losses of void inside the reactors, through the use of laser scattering radiation. On the same collaboration he is analyzing signal acquired from High Resolution Thomson Scattering system (HRTS) at JET in Culham (UK).
From January 2007
Research at University of Rome Tor Vergata.
He is author of 93 papers, 51 articles published on International Journal and Proceedings, one Italian Patent and 28 communications at International and National Congress.
He is a member of European Optical Society since 2004.

A.Malizia

PhD in Quantum Electronics and Plasma Physics. Research field : Analysis of dust mobilization problems in case of Loss of Vacuum Accidents (LOVA) inside fusion nuclear reactors (like ITER), experimental activity. Stager at JET (Joint European Torus) :
•Analysis of Joint European Torus (JET) diagnostics system
•Analysis of Joint European Torus (JET) techniques to manage the components affected by a beryllium contamination
•Analysis of Joint European Torus (JET) procedures and instrumentations used to control loss of vacuum in the plasma chamber.
Consultant in Chemical - Biological- Radiological - Nuclear Protection (CBRN Protection), Didactical Coordinator of Master of Science in " Protection From CBRN events, Tutor in Optical Physics and General Physics.

I.Lupelli:

Ivan Lupelli hold a M.Phil. in Energy Engineer at University of Rome "Tor Vergata", he has worked during a grant in "Business Lab" FILAS Project on development of models for forecasting, monitoring and controlling energy consumption in industrial sector. In his professional career he has worked for engineering company as consulting engineer in mechanical plants, occupational and fire safety (civil and commercials buildings, student residences, industrial buildings, television and radio broadcasting studio). He is Ph.D. candidate in Quantum Electronics and Plasma Physics at University of Rome "Tor Vergata". Specific research topics include numerical simulations of LOVA event and multiphase phenomena in nuclear fusion reactors. Research interests include nuclear fusion safety, energy system, performance-based approach to fire safety design and occupational safety.